Paper 13

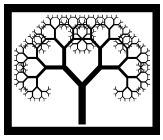

Proceedings of the Eighth International Conference
on Engineering Computational Technology,
B.H.V. Topping, (Editor),
Civil-Comp Press, Stirlingshire, Scotland

Modelling of Moisture Transfer in Soils

T. Krejci and T. Koudelka
Department of Mechanics
Faculty of Civil Engineering
Czech Technical University in Prague, Czech Republic

Abstract

In this paper, a numerical model of the coupled hydro-mechanical behaviour of soils is presented. The micro-mechanics-based model which covers the theory of deformation of soils (soil skeleton) and other porous materials is based on the concept of effective stresses. The final set of equations is simplified and derived for water flow in porous media and the finite element method is used for the spatial discretization. The model was implemented to the SIFEL software package and some numerical examples are presented.

Keywords: moisture transfer, deforming porous medium, soil, pore pressures.

1 Introduction

Soils consists generally from three components - grains (skeleton), liquid (water) and gas (water vapour and air). Total stress in soil can be decomposed to effective stress between grains, pore water pressure and pore gas pressure. Transport of water and heat together with deformation of solid represent non-linear coupled transport problems which can be described by three types of equations. There are constitutive equations (retention curves, material properties), transport equations (Fick's law and Darcy's law) and continuity equations. After discretization of driving equations using finite element method (FEM), a system of non-symmetric and non-linear algebraic equations is obtained generally, even if the deformation of the solid is linear elastic. On the other hand, the moisture transfer is a very slow process and therefore, in case of linear consolidation, no iteration is necessary within time steps. From experiments, it is evident that such a description of consolidation by the linear elastic model for a porous medium along with the constant permeability could not be realistic. At least the permeability is mostly subject of variation reflecting the dependence of the permeability

on void ratio. The Cam-Clay model with the bilinear form of the normal consolidation line (NCL) is then adopted as a suitable model which describes the effect of over-consolidation and structure strength on time dependent processes in soils.

2 Heat and moisture transfer in porous medium

Significant improvement in numerical modelling of coupled heat and moisture transport in porous materials has been attained. There are many material models in the literature that allow for the description of coupled heat and moisture transport. For example, there are phenomenological models based on diffusion [1], [2] and [3]. These models are suitable for numerical simulations and modelling of building structures under common climatic conditions. On the other hand, complex micro-mechanical based models, e.g. Lewis and Schrefler's approach [4] and Tenchev's approach [5], using averaging techniques are applied namely to modelling of concrete structures under high temperature conditions and modelling of soil behaviour.

2.1 Lewis and Schrefler's approach of coupled heat and moisture transfer

2.1.1 Principles of mass and heat transfer - retention curves

Porous materials have the capability of absorbing moisture from an environment of air due to adsorption forces, attracting molecules of vapour to the solid parts of the porous system, and due to the depression of water pressure because of the tension over the concave menisci of the water filled capillaries. Moisture in materials can be therefore present as moist air, water and ice or in some intermediate state as adsorbed phase on the pore walls, respectively. Since it is in general not possible to distinguish the different aggregate states, the water content is defined as the ratio of the total moisture weight to the dry weight of the material [6]. Equilibrium of the water content with its local environment is represented by a retention curve of the material, relating the moisture and the relative humidity h of the surrounding air.

In the transient region II, there is a relationship between the relative humidity, the water content (saturation) and the capillary pressure in the pores [4]

$$p^c = p^g - p^w, \tag{1}$$

where $p^w > 0$ is the pressure of the liquid phase (water).

The pressure of the moist air, $p^g > 0$, in the pore system is usually considered as the pressure in a perfect mixture of two ideal gases - dry air, p^{ga}, and water vapour, p^{gw}, i.e.,

$$p^g = p^{ga} + p^{gw} = \Big(\frac{\rho^{ga}}{M_a} + \frac{\rho^{gw}}{M_w}\Big)TR = \frac{\rho^g}{M_g}TR. \tag{2}$$

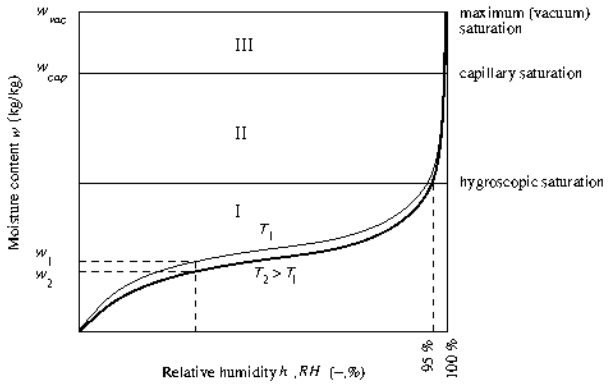

Figure 1: Sorption isotherms

In this relation ρ^{ga}, ρ^{gw} and ρ^g stand for the respective intrinsic phase densities, T is the absolute temperature, and R is the universal gas constant.

Identity (2) defining the molar mass of the moist air, M_g, in terms of the molar masses of individual constituents is known as Dalton's law. The capillary pressure is larger the smaller the capillary radius is. It is shown thermodynamically that the capillary pressure can be expressed unambiguously by the relative humidity h using the Kelvin-Laplace law

$$h = \frac{p^{gw}}{p^{gws}} = \exp\Big(- \frac{p^c M_w}{\rho^w RT}\Big). \tag{3}$$

The water vapour saturation pressure p^{gws} is a function of the temperature only.

Volume fractions of the liquid water (nS_w) and gas (nS_g) (moist air) in porous medium with the porosity n are defined by the following identity

$$(1-n)\rho^s w = nS_w\rho^w + nS_g\rho^g, \qquad S_w + S_g = 1, \tag{4}$$

where the volume moisture w (kg·kg^{-1}) is relate to the water content u (kg.m^{-3}) by the formula

$$u = (1-n)\rho^s w = nS\rho^w + n(1-S)\rho^g = nS(\rho^w - \rho^g) + n\rho^g \tag{5}$$

In soil mechanics, the moisture retention curves are mostly substituted by the material relationship [4]

$$p^c = p^c(S_w, \Theta), \tag{6}$$

again obtained from laboratory tests, where $\Theta = T - T_0$ is the temperature difference above a reference value T_0.

Retention of enthalpy in materials having heat capacities is the term deliberately used to emphasize the similarity to the description of the moisture retention. The retention of enthalpy is simply described as

$$H = H(T), \tag{7}$$

where H is the mass specific enthalpy (J.kg^{-1}), T - temperature (K).

It is not common to write the enthalpy in an absolute way as here. Instead, changes of enthalpy are described in a differential way, which leads to the definition of the specific heat capacity as the slope of the $H - T$ curve, i.e.

$$C_p = \Big(\frac{\partial H}{\partial T}\Big)_{p=\text{const.}}. \tag{8}$$

The heat capacity varies insignificantly with temperature. It is customary, however, to correct this term for the presence of the fluid phases and to introduce the effective heat capacity as

$$\big(\rho C_p\big)_{\text{eff}} = \rho_s C_p^s + \rho_w C_p^w + \rho_g C_p^g. \tag{9}$$

Retention curves reflect material properties of porous media and their descriptions together with Equation (8) are commonly known as the state equations.

2.1.2 Moisture transfer - Darcy's and Fick's laws

The general approach to the coupled moisture and heat transfer in porous media is to express the vector of the mass flux of moisture $\boldsymbol{J}$ and the heat flux vector $\boldsymbol{q}$ as a linear combination of the gradient of free (not chemically bound) pore-water content and of temperature as driving potentials. Off-diagonal phenomenological coefficients of a square (2x2) matrix describing this relation represent cross effects - the Soret flux of moisture and the Dufour flux of heat (see, e.g. [8], [9]). Since gradients $\mathrm{grad}(w)$ and $\mathrm{grad}(T)$ are not the generalized thermo-dynamical forces associated with the fluxes $\boldsymbol{J}$ and $\boldsymbol{q}$, the coefficient matrix is generally non-symmetric. In addition, the water content is not even a continuous potential. That is why a number of modified models have been developed (see, e.g., [8], [1]) considering w as a function of temperature and pore water pressure and assuming that relevant functions are valid for the modified phenomenological coefficients.

If moisture convection is neglected, the liquid and gas (moist air) transport and the vapour diffusion taking place in the gas are the remaining driving mechanisms.

The mass averaged relative velocities, $\boldsymbol{v}^\alpha - \boldsymbol{v}^s$, are expressed by the generalized form of Darcy's law [4]

$$nS_\alpha\big(\boldsymbol{v}^\alpha - \boldsymbol{v}^s\big) = \frac{k^{r\alpha}\boldsymbol{k}_{\text{sat}}}{\mu^\alpha}\big(-\operatorname{grad} p^\alpha + \rho^\alpha \boldsymbol{g}\big), \tag{10}$$

where $\alpha = w$ for the liquid phase and $\alpha = g$ for the gaseous phase. Dimensionless relative permeabilities $k^{r\alpha} \in \langle 0, 1\rangle$ are functions of degree of saturation $k^{r\alpha} = k^{r\alpha}(S_w)$. $\boldsymbol{k}_{\text{sat}}$ (m^2) is the square (3x3) intrinsic permeability matrix and μ^α is the dynamic viscosity (kg.m^{-1}s^{-1}). The intrinsic mass densities ρ^α are related to the volume averaged mass densities ρ_α through the relation

$$\rho_\alpha = nS_\alpha \rho^\alpha. \tag{11}$$

Diffusive-dispersive mass flux (kg.m^{-2}s^{-1}) of the water vapour (gw) in the gas (g) is the second driving mechanism. It is governed by Fick's law

$$\boldsymbol{J}_g^{gw} = nS_g\rho^{gw}\big(\boldsymbol{v}^{gw} - \boldsymbol{v}^g\big) = -\rho^g \boldsymbol{D}_g^{gw}\mathrm{grad}\Big(\frac{\rho^{gw}}{\rho^g}\Big), \tag{12}$$

where $\boldsymbol{D}_g^{gw}$ (m^2.s^{-1}) is the effective dispersion tensor. It can be shown [4] that

$$\boldsymbol{J}_g^{gw} = -\rho^g \frac{M_a M_w}{M_g^2}\boldsymbol{D}_g^{gw}\mathrm{grad}\Big(\frac{\rho^{gw}}{\rho^g}\Big) = \rho^g \frac{M_a M_w}{M_g^2}\boldsymbol{D}_g^{ga}\mathrm{grad}\Big(\frac{\rho^{ga}}{\rho^g}\Big) = -\boldsymbol{J}_g^{ga}. \tag{13}$$

Recall that $\boldsymbol{D}_g^{gw} = \boldsymbol{D}_g^{ga} = \boldsymbol{D}_g$. Here, $\boldsymbol{J}_g^{ga}$ is the diffusive-dispersive mass flux of the dry air in the gas.

There is a number of models based on the assumption, where the water vapour is considered to be the only component of the gas and Darcy's law (10) is used to describe the motion of the liquid phase as well as of the water vapour (see, e.g., [7]). In such a case, Equation (10) is valid for upper scripts $\alpha = w, gw$ and corresponding expressions for the respective mass fluxes of these components in the solid assume the form

$$\begin{aligned}\boldsymbol{J}_s^\alpha = nS_\alpha\rho^\alpha\big(\boldsymbol{v}^\alpha - \boldsymbol{v}^s\big) = \frac{\boldsymbol{K}^\alpha}{g}\big(-\mathrm{grad}\,p^\alpha + \rho^\alpha\boldsymbol{g}\big) = \\ = \frac{k^{r\alpha}\boldsymbol{k}_{\mathrm{sat}}}{\nu^\alpha}\big(-\mathrm{grad}\,p^\alpha + \rho^\alpha\boldsymbol{g}\big), \quad \alpha = w, gw,\end{aligned} \tag{14}$$

where $\nu^\alpha = \mu^\alpha/\rho^\alpha$ (m^2.s^{-1}) is the kinematic viscosity of α component. For the liquid transport, $\boldsymbol{K}^w/g$ (s) is called hydraulic conductivity (g is acceleration of gravity).

The fluid is also transferred across interfaces with the surrounding environment by means of convection fluxes $\boldsymbol{J}_c^\alpha, \alpha = w, wg$, that can be expressed by the following boundary conditions for liquid water

$$\overline{q}^w = \boldsymbol{\nu}^T\boldsymbol{J}_c^w = \boldsymbol{\nu}^T\rho^w\frac{k^{rw}\boldsymbol{k}_{sat}}{\mu^w}\big(-\mathrm{grad}\,p^w + \rho^w\boldsymbol{g}\big), \quad \text{on} \quad \Gamma^w, \tag{15}$$

and for the water vapour on Γ^{gw}

$$\overline{q}^{gw} = \boldsymbol{\nu}^T\boldsymbol{J}_c^{gw} = \boldsymbol{\nu}^T\rho^{gw}\frac{k^{rgw}\boldsymbol{k}_{sat}}{\mu^{gw}}\big(-\mathrm{grad}\,p^{gw} + \rho^{gw}\boldsymbol{g}\big) = \beta^{gw}\big(p_{\mathrm{surf}}^{gw} - p_{\mathrm{air}}\big), \tag{16}$$

where β^{gw} (s.m^{-1}) is the convection mass transfer coefficient, p_{surf}^{gw} is the surface water vapour pressure and p_{air} is the water vapour pressure of surrounding air.

2.1.3 Transfer of heat - Fourier's law

Conduction in normal sense comprises radiation as well as convective heat transfer on a microscopic level. The generalized version of Fourier's law is used to describe the conduction heat transfer

$$\boldsymbol{q} = -\boldsymbol{\chi}_{\mathrm{eff}}\mathrm{grad}\,T, \tag{17}$$

where $\boldsymbol{q}$ is the heat flux (W.m^{-2}), $\boldsymbol{\chi}_{\text{eff}}$ is the effective thermal conductivity matrix (W.m^{-1}.K^{-1}).

The outer surface exchange heat can be expressed by convection and thermal radiation

$$\boldsymbol{\nu}^T \boldsymbol{q} = (\beta_c + \beta_r(T))(T_{\text{surf}} - T_{\text{air}}) + \beta_c \boldsymbol{\nu}^T \boldsymbol{J}_c^{gw}, \tag{18}$$

where β_c is the heat transfer coefficient and β_r is the radiation heat coefficient. The last term is the heat loss due to latent heat of moisture vaporization at the surface.

2.1.4 Mass and energy balance equation

In addition to the constitutive equations, the mass and energy balance equations are needed to complete a set of equations describing the mass and heat transfer. The balance equations are based on the assumptions of extended Biot's theory.

Starting from the mass balance equation for the solid

$$\frac{\partial\big[(1-n)\rho^s\big]}{\partial t} + \operatorname{div}\big[(1-n)\rho^s \boldsymbol{v}^s\big] = 0. \tag{19}$$

The corresponding equations for the fluid phases assume this form for liquid water

$$\frac{\partial\big(nS_w\rho^w\big)}{\partial t} + \operatorname{div}\big[nS_w\rho^w \boldsymbol{v}^w\big] = -\dot{m}, \tag{20}$$

and for gas

$$\frac{\partial\big[n(1-S_w)\rho^g\big]}{\partial t} + \operatorname{div}\big[n(1-S_w)\rho^g \boldsymbol{v}^g\big] = \dot{m}, \quad S_g + S_w = 1, \tag{21}$$

where $\dot{m}$ is the mass rate of evaporation, $\partial/\partial t$ is the time derivative.

Writing Equation (21) for superscript gw instead of g and then using Equation (12), the following form of the mass balance equation for the vapour phase is obtained:

$$\frac{\partial\big[n(1-S_w)\rho^{gw}\big]}{\partial t} + \operatorname{div}\boldsymbol{J}_g^{gw} + \operatorname{div}\big[n(1-S_w)\rho^{gw}\boldsymbol{v}^{gw}\big] = \dot{m}. \tag{22}$$

Equations (19) through (22) can be rearranged in different manners. A starting point is elimination of the time derivative of the porosity by means of Equation (19). Substitution of this term into Equation (20) and Equation (21) gives the continuity equations of the liquid water and gas.

When dealing with the phase change, it is more convenient to express the energy balance by means of the specific enthalpy. If some insignificant terms are neglected and providing the local equilibrium state holds $\big(T^\alpha = T, \text{ for } \alpha = s, w, g\big)$, the energy balance equation leads to the following form [4]

$$\big(\rho C_p\big)_{\text{eff}} \frac{\partial T}{\partial t} + \big(\rho_s C_p^s \boldsymbol{v}^s + \rho_w C_p^w \boldsymbol{v}^w + \rho_g C_p^g \boldsymbol{v}^g\big)\operatorname{grad} T = -\operatorname{div}\boldsymbol{q} - \dot{m}\Delta H^{gw}, \tag{23}$$

where $\Delta H^{gw} = H^{gw} - H^{w}$ is the latent heat of evaporation, the convective heat flux in the solid phase $\rho_s C_p^s \boldsymbol{v}^s = \big(1-n\big)\rho^s C_p^s \boldsymbol{v}^s$ is usually neglected. The convective heat fluxes due to movement of the fluid $\rho_w C_p^w \boldsymbol{v}^w$ and $\rho_g C_p^g \boldsymbol{v}^g$ can be usually neglected as well. But in rapid heating this might not be true. In some cases, further source terms should be introduced in addition to the heat due evaporation (e.g., the heat of dehydration of concrete).

3 Deformation of solid skeleton

3.1 Concept of effective stresses

The stresses in the grains, $\boldsymbol{\sigma}^s$, can be expressed using a standard averaging technique in terms of the stresses in the liquid phase, $\boldsymbol{\sigma}^w$, the stresses in the gas, $\boldsymbol{\sigma}^g$, and the effective stresses between the grains, $\boldsymbol{\sigma}^{ef}$. The equivalence condition for the internal stresses leads to [10]

$$(1-n)\boldsymbol{\sigma}^s = (1-n)S_w\boldsymbol{\sigma}^w + (1-n)S_g\boldsymbol{\sigma}^g + \boldsymbol{\sigma}^{ef} \tag{24}$$

similarly, the total stress can be expressed as

$$\boldsymbol{\sigma} = nS_w\boldsymbol{\sigma}^w + nS_g\boldsymbol{\sigma}^g + (1-n)\boldsymbol{\sigma}^s + \Delta\tau, \tag{25}$$

where $\Delta\tau$ is the surface traction on the surface between the liquid and the gas phase of neighbouring volumes. Combining Equations (24) and (25) gives

$$\boldsymbol{\sigma} = \boldsymbol{\sigma}^{ef} + S_w\boldsymbol{\sigma}^w + S_g\boldsymbol{\sigma}^g + \Delta\tau. \tag{26}$$

Assuming negligible shear stress in fluids, Equation 26 takes the form

$$\boldsymbol{\sigma} = \boldsymbol{\sigma}^{ef} - p^s\boldsymbol{m}, \tag{27}$$

where $\boldsymbol{m} = \{1,1,1,0,0,0\}^{\mathrm{T}}$ and $p^s = S_w p^w + S_g p^g$. Deformation of a porous skeleton associated with the grain rearrangement can be expressed using the constitutive equation written in the rate form

$$\dot{\boldsymbol{\sigma}}^{ef} = \boldsymbol{D}_{sk}(\dot{\boldsymbol{\varepsilon}} - \dot{\boldsymbol{\varepsilon}}_0). \tag{28}$$

The dots denote differentiation with respect to time, $\boldsymbol{D}_{sk} = \boldsymbol{D}_{sk}(\dot{\boldsymbol{\varepsilon}}, \boldsymbol{\sigma}^{ef}, T)$ is the tangential matrix of the porous skeleton and $\dot{\boldsymbol{\varepsilon}}_0$ represents the strains that are not directly associated with stress changes (e.g., temperature effects, shrinkage, swelling, creep). It also involves the strain of the bulk material due to changes of the pore pressure

$$\dot{\boldsymbol{\varepsilon}}_{pp} = -\boldsymbol{m}\Big(\frac{\dot{p}^s}{3K_s}\Big), \tag{29}$$

where K_s is the bulk modulus of the solid material (matrix).

When admitting only this effect and combining Equations (27), (28) and (29), the following equation is obtained

$$\dot{\boldsymbol{\sigma}} = \dot{\boldsymbol{\sigma}}^{ef} - \dot{p}^s \boldsymbol{m} = \boldsymbol{D}_{sk}\dot{\boldsymbol{\varepsilon}} - \alpha \boldsymbol{m}\dot{p}^s, \tag{30}$$

where α is the Biot's constant.

It has to be point out that changes of the effective stress along with temperature and pore pressure changes produce change of the solid density $\dot{\rho}_s$. This quantity can be obtained from the mass conservation equation for the solid phase and the derivation in detail can be found literature, e.g. in [4] and [6].

3.2 Set of governing equations

The complete set of equations describing the coupled moisture and heat transport in deforming porous media comprises the linear balance (equilibrium) equation formulated for a multiphase body, the energy balance equation and the continuity equations for the liquid water and gas. The continuity equation for the liquid phase can be derived from the balance equation (20) converted by means of Equations (19), (23) and by neglecting the gradient of $(1-n)\rho^s$

$$\frac{\alpha - n}{K_s}\frac{\partial}{\partial t}\left(S_w p^w + S_g p^g\right) + n\frac{\dot{p}^w}{K_w} - [(\alpha - n)\beta_s + n\beta_w]\dot{T} + n\frac{\dot{S}^w}{S_w}\alpha \mathrm{div}\boldsymbol{v}^s + \frac{1}{S_w p^w}\mathrm{div}\boldsymbol{J}_s^w = -\frac{\dot{m}}{S_w \rho^w}, \tag{31}$$

where the flux of the liquid water in the solid is expressed by Darcy's law (10). The continuity equation for gas is derived in a similar manner by modifying the balance equation (22) and using Equation (2) to eliminate $\dot{\rho}^g$. The final result is:

$$\frac{\alpha - n}{K_s}\frac{\partial}{\partial t}\left(S_w p^w + S_g p^g\right) + n\frac{\dot{p}^w}{K_w} - (\alpha - n)\beta_s \dot{T} + \frac{n}{\rho^g}\frac{\partial}{\partial t}\left[\frac{p^g M_g}{TR}\right]\alpha \mathrm{div}\boldsymbol{v}^s + \frac{1}{S_g p^g}\mathrm{div}\boldsymbol{J}_s^g = +\frac{\dot{m}}{S_g \rho^g}. \tag{32}$$

The flux of gas is expressed by Equation (14) written for $\alpha = g$. The equilibrium equation (the linear balance equation) must yet be introduced to complete a set of governing equations. Neglecting inertia forces and the convective terms simplifies this equation into the well-known form

$$\mathrm{div}\boldsymbol{\sigma} + \rho \boldsymbol{g} = 0, \tag{33}$$

with density of the multiphase medium defined as

$$\rho = (1-n)\rho^s + nS_w\rho^w + nS_g\rho^g = \rho_s + \rho_w + \rho_g. \tag{34}$$

The fundamental unknowns in the theory of the coupled moisture and heat transport are represented by the pressures in the liquid and gas phase, respectively, p^w, p^g; the

temperature T; the vector of the displacement rate, $\boldsymbol{v}^s$, of the solid phase. The six unknown functions, defined in a domain Ω with a boundary Γ , can be solved from 6 basic equations - two continuity equations (31) and (32), one energy balance equation (23) and the equilibrium equations written in the vectorial form (33). Saturation S_w and $S_g = 1 - S_w$ can be eliminated by means of the retention formula (1) in conjunction with relation (6). The fluxes J_{sw} and J_{sg} are expressed using Darcy's law (10).

3.3 Saturated-unsaturated one-phase flow in a deforming medium

3.3.1 Fundamental equations

Most processes of consolidation in soils are taking place at constant temperature, moreover, the water flow is often the only driving mechanism of moisture transfer. For this case, the assumption of isothermal one-phase flow is adopted. Since a zero pressure of the moist air, $p^g = 0$, is supposed, the continuity equation (32) for the gaseous phase can be omitted and remaining equations can be simplified.

The continuity equation (31) for the liquid phase is rearranged as

$$\Big(\frac{\alpha - n}{K_s} S_w^2 + n\frac{nS_w}{K^w}\Big)\dot{p}^w + \Big(\frac{\alpha - n}{K_s} S_w p^w + n\Big)\dot{S}_w + \alpha S_w \mathrm{div}\boldsymbol{v}^s + \frac{1}{\rho^w}\mathrm{div}\boldsymbol{J}_s^w = 0. \tag{35}$$

For fully saturated one-phase flow, the continuity equation can reduced by taking $S_w = 1$, $k^{rw} = 1$ and $\partial S_w/\partial p^w = 0$.

The linear momentum balance equation (33) (equation of equilibrium),

$$\mathrm{div}\boldsymbol{\sigma} + \rho\boldsymbol{g} = 0, \tag{36}$$

is expressed in terms of the total stresses with density of the multiphase medium $\rho = (1-n)\rho^s + nS_w\rho^w = \rho_s + \rho_w$, and total stresses

$$\boldsymbol{\sigma} = \boldsymbol{\sigma}'' - \alpha \boldsymbol{m} S_w p^w, \tag{37}$$

where $\boldsymbol{\sigma''} = \boldsymbol{D}_{\mathrm{sk}}\boldsymbol{\varepsilon}$ is the generalized effective stress defined by Equation (30) to account for the deformation of grains.

Finally, the suitable substitution of Darcy's law (10) and the relation $\mathrm{div}\boldsymbol{v}^s = \boldsymbol{m}^{\mathrm{T}}\boldsymbol{\varepsilon}$ in Equation (31) leads to its following expression

$$\Big(\frac{\alpha - n}{K_s} S_w^2 + \frac{nS_w}{K^w}\Big)\dot{p}^w + \Big(\frac{\alpha - n}{K_s} S_w p^w + n\Big)\dot{S}_w + \alpha S_w \boldsymbol{m}^{\mathrm{T}}\partial^{\mathrm{T}}\dot{\boldsymbol{u}} + \nabla^{\mathrm{T}}\Big[\frac{k^{rw}\boldsymbol{k}_{\mathrm{sat}}}{\mu^w}(-\nabla p^w + \rho^w \boldsymbol{g})\Big] = 0, \tag{38}$$

where the fundamental unknowns are represented by the scalar field of pore water pressure p^w and the vector field of displacements $\boldsymbol{u} = \{u, v, w\}^{\mathrm{T}}$.

3.3.2 Numerical solution

Applying Galerkin's method, the Gauss theorem and using the spatial discretization with the usual approximation of the displacement field and the pore water pressure

$$\boldsymbol{u} = \boldsymbol{N}_u \boldsymbol{d}_u, \tag{39}$$

$$p^w = \boldsymbol{N}_p \boldsymbol{d}_p. \tag{40}$$

the system of equations for the hydro-mechanical problem (cf. [4], [10]) is obtained

$$\begin{pmatrix} \boldsymbol{0} & \boldsymbol{0} \\ \boldsymbol{C}_{pu} & \boldsymbol{C}_{pp} \end{pmatrix} \begin{pmatrix} \dot{\boldsymbol{d}}_u \\ \dot{\boldsymbol{d}}_p \end{pmatrix} + \begin{pmatrix} \boldsymbol{K}_{uu} & \boldsymbol{K}_{up} \\ \boldsymbol{0} & \boldsymbol{K}_{pp} \end{pmatrix} \begin{pmatrix} \boldsymbol{d}_u \\ \boldsymbol{d}_p \end{pmatrix} = \begin{pmatrix} \boldsymbol{f}_u \\ \boldsymbol{f}_p \end{pmatrix}, \tag{41}$$

with following matrices:
the stiffness matrix

$$\boldsymbol{K}_{uu} = \int_\Omega \boldsymbol{B}_u^{\mathrm{T}} \boldsymbol{D} \boldsymbol{B}_u \, \mathrm{d}\Omega, \tag{42}$$

the permeability matrix

$$\boldsymbol{K}_{pp} = \int_\Omega (\nabla \boldsymbol{N}_p)^{\mathrm{T}} \frac{k^{rw} \boldsymbol{k}_{\mathrm{sat}}}{\mu^w} \nabla \boldsymbol{N}_p \, \mathrm{d}\Omega, \tag{43}$$

the compressibility matrix

$$\boldsymbol{C}_{pp} = \int_\Omega \boldsymbol{N}_p^{\mathrm{T}} \Big(\frac{\alpha - n}{K_s} S_w \big(S_w + \frac{\partial S_w}{\partial p^w} p^w \big) + n \big(\frac{\partial S_w}{\partial p^w} + \frac{S_w}{K_w} \big) \Big) \boldsymbol{N}_p \, \mathrm{d}\Omega \tag{44}$$

and the coupling matrices

$$\boldsymbol{K}_{up} = -\int_\Omega \boldsymbol{B}_u^{\mathrm{T}} \alpha S_w \boldsymbol{m}^{\mathrm{T}} \boldsymbol{N}_p \, \mathrm{d}\Omega, \tag{45}$$

$$\boldsymbol{C}_{pu} = \int_\Omega \boldsymbol{N}_p^{\mathrm{T}} \alpha S_w \boldsymbol{m}^{\mathrm{T}} \boldsymbol{B}_u \, \mathrm{d}\Omega. \tag{46}$$

The right-hand side terms are:
the force vector

$$\boldsymbol{f}_u = \int_\Omega \boldsymbol{N}_u^{\mathrm{T}} \rho \boldsymbol{g} \, \mathrm{d}\Omega + \int_{\Gamma_t} \boldsymbol{N}_u^{\mathrm{T}} \boldsymbol{t} \, \mathrm{d}\Gamma, \tag{47}$$

and the flow vector

$$\boldsymbol{f}_p = \int_\Omega (\nabla \boldsymbol{N}_p)^{\mathrm{T}} \frac{k^{rw} \boldsymbol{k}_{\mathrm{sat}}}{\mu^w} \rho \boldsymbol{g} \, \mathrm{d}\Omega - \int_{\Gamma_w} \boldsymbol{N}_u^{\mathrm{T}} \frac{\overline{q}^w}{\rho^w} \, \mathrm{d}\Gamma. \tag{48}$$

For the sake of consistency, it is convenient to approximate the strains $\boldsymbol{\varepsilon}$ and the pore water pressure p^w by polynomials of the same degree. Strain-displacement equations then imply that the displacements are to be approximated by a polynomial one order higher than the pore pressure.

The system of differential equations (41) has to be solved by an incremental method. Time discretization is based on the v-form of the generalised trapezoidal method [11]. The resulting system of algebraic equations is generally non-linear and the Newton-Raphson method [10] has to be used at each time step.

4 Numerical examples

4.1 Sand desaturation - a benchmark problem for non-saturated flow

The presented benchmark is based on an experiment performed by Liakopoulos [12] on a column of Del Monte sand [4]. This test problem has been solved previously by many authors to check their numerical models, e.g, Liakopoulos [12], Schrefler and Simoni [13], Zienkiewicz et al. [14], Schrefler and Zhan [15], Gawin and Schrefler [16], as well as Lewis and Schrefler [4].

Young's modulus	E = 13 MPa
Poisson's ration	ν = 0.4
Biot's constant	α = 1
Solid grain density	ρ^s = 2000 kg·m^{-3}
Liquid density	ρ^w = 1000 kg·m^{-3}
Poisson's ration	ν = 0.4
Porosity	n_0 = 0.2975
Intrinsic permeability	k_{sat} = 4.5 $\times$ 10^{-13} m^2
Water viscosity	μ^w = 1 $\times$ 10^{-3} Pa·s
Air viscorisy	μ^g = 1.8 $\times$ 10^{-5} Pa·s
Gravitational acceleration	g = 9.806 m·s^{-2}
Saturation	$S = 1 - 1.9722 \times 10^{-11} p^{c2.4279}$, for $S \geq 0.91$
Relative permeability	$k^{rw} = 1 + 2207(1 - S)^{1.0121}$, for $S \geq 0.91$
Relative permeability of the gas phase	$k^{rg} = (1 - S_e)^2(1 - S_e^{5/3})$ $S_e = (S - 0.2)/(1 - 0.2)$
Time increment	Δt = 10 s

Table 1: Material properties for the Liakopoulos test problem

In this example, partially saturated flow in deforming porous media is investigated under the assumption that, either air remains at atmospheric pressure in the unsaturated zone, or there is flow of both water and air. In this Liakopoulos test, the sand column was continuously added by water from the top and allowed to drain freely at the bottom through a filter, until uniform flow conditions were established. The material properties and parameters are given in Table 1 and the experiment set up is shown in Figure 2.

The problem was solved as one-phase flow, where the gas pressure was assumed equal to the atmospheric pressure in the partially saturated zone, as well as two-phase flow with switching at $p^c = 2000$ Pa ($S = 0.998$, no gas flow below the bubble point pressure) and an additional lower limit for the gas relative permeability of $k_{rg,\min} = 0.0001$ [4]. The transition from a fully saturated state to a partial saturated state during the desaturation process is secured by a switching process at certain value close to

saturation $S_w = 1$, which is corresponding to the bubbling pressure, which has a physical justification. The application of an additional lower limit for the gas relative permeability is necessary to avoid oscillations in the pressure solution [16]. Both methods of solution gave nearly the same results.

For numerical calculations, the column of soil was divided into 10 isoparametric quadrilateral (2D) finite elements with linear approximation functions. The benchmark was solved by SIFEL software [17], [18], where the algorithm for coupled heat and moisture transfer in deforming porous medium was implemented. SIFEL (Simple Finite Elements) computer code is being developed at the Department of Structural Mechanics at Faculty of Civil Engineering at Czech Technical University in Prague. The code is written in the C++ language and can be found at the web address [19]. Results of computation are shown in Figure 3.

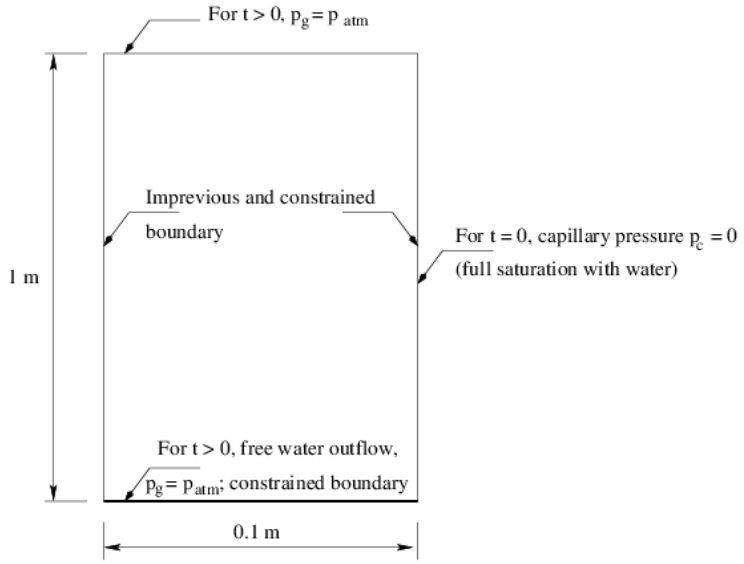

Figure 2: The Liakopoulos test problem

4.2 Isothermal consolidation

A simple 2D benchmark of a soil consolidation under loaded basement is another example which illustrates the moisture transfer in deforming porous medium. In this case, the assumption of fully saturated porous media is adopted. The setting of the benchmark with hydrostatic water pressure as the initial condition and loading evolution are shown in Figure 4 with soil parameters: Youngs modulus $E = 10$ MPa; Poissons ratio $\nu = 0.4$; bulk modulus of the solid material K_s = 18000 MPa; bulk modulus of the porous skeleton K_{sk} = 3.6 MPa; porosity n = 0.5; permeability $\frac{k^{rw} k_{\mathrm{sat}}}{\mu^w}$ = $1.1574 \cdot 10^{-8}$ m^2/s. Selected results are depicted in Figure 5, where the time evolution of vertical displacement under the loaded basement shows the very slow consolidation process.

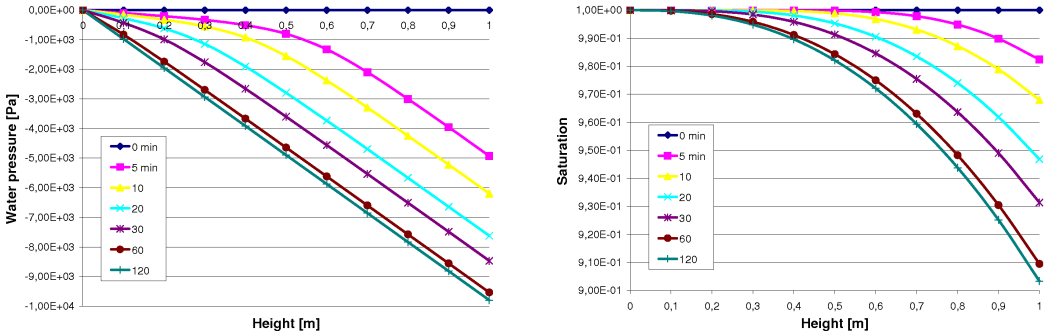

Figure 3: Water pressure (left) and saturation (right) versus height

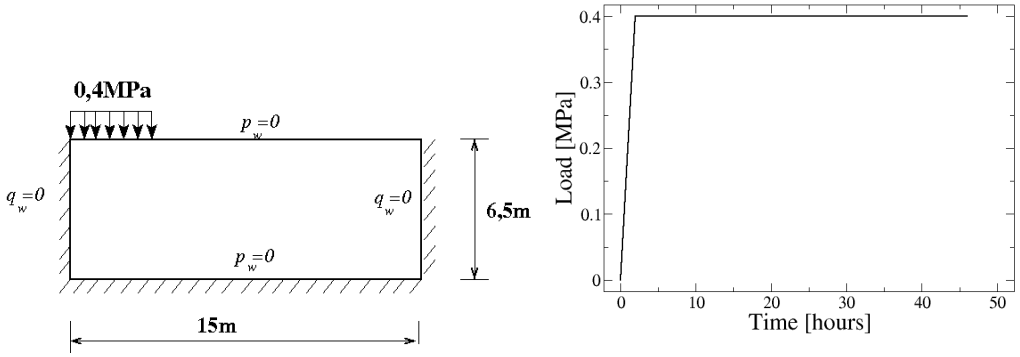

Figure 4: Benchmark settings and loading

5 Variation of permeability - Cam-Clay model

There exists, however, experimental evidence that such a description of consolidation by the linear elastic model for a porous medium along with the constant permeability could not be realistic. At least the permeability is mostly subject of variation. Some formulas reflecting the dependence of the permeability on void ratio, $e = n/(1-n)$ can be found in literature, where the Cam-Clay model seems to be suitable for modelling of cohesive soils and it was used to confront the results obtained theoretically and from triaxial tests [20].

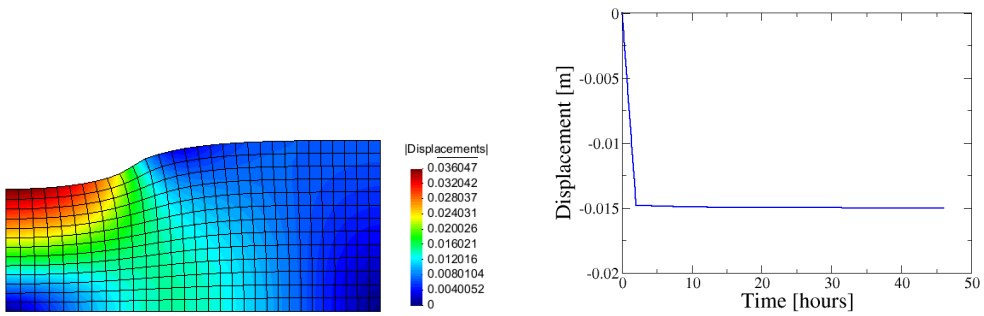

Figure 5: Deformation of soil (left) and time evolution of vertical displacement under the basement (right)

5.1 Cam-Clay plasticity model

The modified Cam-Clay model is an hardening/softening elastoplastic model where the hardening/softening behaviour is governed by volumetric plastic strain. The yield criterion represents envelopes which are self-similar in shape and they correspond to ellipsoids with rotation about the mean stress axis in the principal stress space. The shear flow rule is associated and no resistance to tensile stress is assumed in this model. The model was proposed by [21] originally and more details about the model can be also found in [22].

The model is expressed in terms of three variables: the mean stress σ_m, the deviatoric stress q and specific volume v. The quantities connected with stress state are defined with help of stress tensor invariants as follows

$$\sigma_m = \frac{1}{3}\sigma_{ii}, \tag{49}$$

$$s_{ij} = \sigma_{ij} - \delta_{ij}\sigma_m, \tag{50}$$

$$q = \sqrt{\frac{3}{2}s_{ij}s_{ij}}, \tag{51}$$

where δ_{ij} is the Kronecker delta. The specific volume v can be given by the ratio of the total volume V and volume of solid particles V_s, using the the void ratio e or with help of volumetric strain ε_v

$$v = \frac{V}{V_s} = 1 + e = v_0(1 + \varepsilon_v), \tag{52}$$

$$\varepsilon_v = \varepsilon_{ii}. \tag{53}$$

where v_0 is the initial specific volume. Assuming above relations, the yield function f has the form

$$f(\sigma_{ij}) = q^2 + M^2\sigma_m(\sigma_m - p_c), \tag{54}$$

where p_c is the hardening parameter, also called the pre-consolidation pressure, which determines the diameter of the ellipsoid along the σ_m axis. The material parameter M influences the slope of the critical state line and consequently, the radius of the ellipsoid in the deviatoric plane. The ellipsoidal yield surface for this criterion is defined by the yield condition such that

$$f(\boldsymbol{\sigma}, p_c) = 0. \tag{55}$$

The section of the yield surface in the $p - q$ plane is depicted in Figure 6.

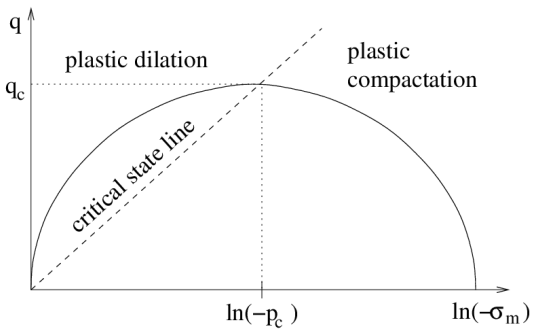

Figure 6: Cam-Clay yielded surface in $p - q$-plane

The Cam-Clay model reflects a non-linear law derived experimentally from isotropic compression tests. The results of a typical isotropic compression test is presented in the semi-logarithmic plot in Figure 7.

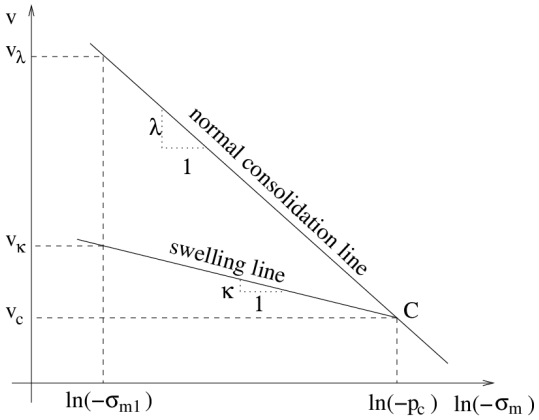

Figure 7: Normal consolidation and swelling lines for an isotropic compression test

In Figure 7 can be observed that as the consolidation pressure σ_m increases, the specific volume v decreases and the point representing the actual state of the material moves along the normal consolidation line whose slope is given by the another material parameter λ. The NCL line can be expressed by the following relation

$$v = v_\lambda - \lambda \ln \frac{\sigma_m}{\sigma_{m1}}, \tag{56}$$

where σ_{m1} is the reference pressure and the v_λ is the initial specific volume at the reference pressure σ_{m1}.

The swelling line captures elastic unloading excursions from point C and its slope is given by the material parameter κ. Reloading will move the point along the elastic swelling line until the normal consolidation line is reached and then it continues along the normal consolidation line. The equation of the swelling line has the form

$$v = v_\kappa - \kappa \ln \frac{\sigma_m}{\sigma_{m1}}, \tag{57}$$

where the value v_κ for a particular swelling lines depends on the location of the point on the normal consolidation line, from which the unloading was performed.

Rewriting Equations (56) and (57) for point C (see Figure 7) yields

$$-\kappa = \frac{v_c - v_\kappa}{\ln(-p_c) - \ln(-\sigma_{m1})}, \quad -\lambda = \frac{v_c - v_\lambda}{\ln(-p_c) - \ln(-\sigma_{m1})}. \tag{58}$$

It should be noted that the λ and κ values are assumed to be positive. Combining Equations (58) the hardening/softening rule can be obtained in the form

$$p_c = \sigma_{m1} \exp\left(\frac{v_\lambda - v_\kappa}{\lambda - \kappa}\right), \tag{59}$$

where p_c is the pre-consolidation pressure which represents the maximum value of the mean stress σ_m attained in the loading history.

The material parameter M is related to the friction angle ϕ and it also depends on the type of loading. It is assumed to be $M = 6\sin(\phi)/(3 - \sin(\phi))$ for triaxial compression test and $M = 6\sin(\phi)/(3 + \sin(\phi))$ for triaxial extension test.

Should be noted that in the case of effective stress concept, all stress quantities have to be computed from the effective stress tensor $\boldsymbol{\sigma}^{ef}$ instead of total one.

Plastic materials are characterized by the evolution of irreversible deformations upon unloading. Additionally, it is assumed that the behaviour of these materials is elastoplastic which means that the slopes of the stress-strain diagram for unloading are identical with the initial elastic slope. The total strain can be decomposed as follows

$$\boldsymbol{\varepsilon} = \boldsymbol{\varepsilon}_e + \boldsymbol{\varepsilon}_p \tag{60}$$

where $\boldsymbol{\varepsilon}$ is the total strain, $\boldsymbol{\varepsilon}_e$ is the elastic reversible strain and $\boldsymbol{\varepsilon}_p$ is the plastic irreversible strain. The stresses can be calculated with help of elastic strains according to the linear elasticity law

$$\boldsymbol{\sigma} = \boldsymbol{D}_e \boldsymbol{\varepsilon}_e, \tag{61}$$

where $\boldsymbol{D}_e$ is the initial elastic stiffness matrix. The evolution of plastic strains can be defined with help of associated plastic flow rule which is defined by the expression

$$\dot{\boldsymbol{\varepsilon}}_p = \dot{\gamma} \frac{\partial f}{\partial \boldsymbol{\sigma}}, \tag{62}$$

where $\dot{\gamma}$ is the rate of plastic multiplier or consistency parameter, which controls the magnitude of the plastic strain $\boldsymbol{\varepsilon}_p$. This evolution rule represents differential equation which cannot be integrated in the closed form generally. There are many numerical integration schemes providing approximate solution which are called stress return algorithms in plasticity (see, e.g., [23], [24], [25]). If the cutting plane algorithm is adopted for the integration of the flow rule in the Cam-Clay model, the following derivatives are necessary

$$\frac{\partial f}{\partial \sigma_{ij}} = 3s_{ij} + \frac{1}{3}M^2\delta_{ij}(\frac{2}{3}\sigma_{kk} - p_c), \tag{63}$$

$$\frac{\partial f}{\partial p_c} = -M^2\sigma_m, \tag{64}$$

$$\frac{\partial p_c(\boldsymbol{\varepsilon}_p)}{\partial \gamma} = p_c\left(\frac{v_0}{\lambda-\kappa}\right)\frac{\partial \varepsilon_{vp}}{\partial \gamma}, \tag{65}$$

$$\frac{\partial \varepsilon_{vp}}{\partial \gamma} = M^2(2\sigma_m - p_c), \tag{66}$$

where ε_{vp} is the volumetric plastic strain which is given by inner product of the plastic strain tensor $\boldsymbol{\varepsilon}_p$ and Kronecker delta $\varepsilon_{vp} = \boldsymbol{\varepsilon}_p : \boldsymbol{\delta}$.

5.2 Variation of permeability

To describe the way, in which the over-consolidation and structure strength influence time dependent processes in soils, the bilinear form of the normal consolidation line (NCL) will be adopted (Figure 7). Both the theoretical and experimental solutions will be curried out for the simplest case of uni-axial one-phase flow in a fully saturated medium. In this case, The governing continuity equation (mass balance) reads

$$-\frac{\partial}{\partial z}\left(\frac{K}{\gamma^w}\frac{\partial p^w}{\partial z}\right) + \dot{\varepsilon}_v = 0, \tag{67}$$

where K is the permeability appeared in the hydraulic conductivity K^w/g in Equation (14), $\gamma^w = g\rho^w$ is the specific weight of water, and $\dot{\varepsilon}_v$ represents the rate of volumetric strain expressed generally as $\dot{\varepsilon}_v = \mathrm{div}\boldsymbol{v}^s = \boldsymbol{m}^{\mathrm{T}}\dot{\boldsymbol{\varepsilon}}$. In case of cohesive soils, it is convenient to set $\alpha = 1$ and to neglect gravity term $\rho^w g$ due to the insignificant height of samples.

The equation based on the Cam-Clay model is applied to express the rate of volumetric strain $\dot{\varepsilon}_v$ in terms of the mean effective stress

$$\dot{\varepsilon}_v = -\frac{\lambda}{v_\lambda}\frac{\dot{\sigma}_m^{ef}}{\sigma_m^{ef}}, \tag{68}$$

where σ_m^{ef} stands for the mean effective stress. Eliminating $\dot{\varepsilon}$ is firmly rooted with the assumption that the chamber pressure is constant, i.e.,

$$\dot{\sigma}_m = \dot{\sigma}_m^{ef} - \dot{p}^w = 0 \Rightarrow \dot{\sigma}_m^{ef} = \dot{p}^w. \tag{69}$$

The resulting equation assumes this form

$$\frac{\partial \sigma_m^{ef}}{\partial t} = \frac{v_\lambda}{\lambda} \sigma_m^{ef} \frac{\partial}{\partial z} \left(\frac{K}{\gamma^w} \frac{\partial p^w}{\partial z} \right). \tag{70}$$

For general stress state and the three dimensional moisture transfer with respect to changing permeability, the permeability matrix (42) and the flow vector (48) are changed:

$$\boldsymbol{K}_{pp} = \int_\Omega (\nabla \boldsymbol{N}_p)^{\mathrm{T}} \frac{v_\lambda}{\lambda} \sigma_m^{ef} \frac{K}{\gamma^w} \nabla \boldsymbol{N}_p \, \mathrm{d}\Omega, \tag{71}$$

$$\boldsymbol{f}_p = \int_\Omega (\nabla \boldsymbol{N}_p)^{\mathrm{T}} \frac{v_\lambda}{\lambda} \sigma_m^{ef} \frac{K}{\gamma^w} \rho \boldsymbol{g} \, \mathrm{d}\Omega - \int_{\Gamma_w} \boldsymbol{N}_p \frac{\overline{q}^w}{\rho^w} \, \mathrm{d}\Gamma. \tag{72}$$

It has been verified experimentally that in case of uni-axial consolidation a mere power law written as [20]

$$\frac{K}{K_0} = \left(\frac{v}{v_\lambda} \right)^m, \tag{73}$$

represents the soil behaviour fairly well. Parameter m is yet to be determined to match numerical solution of Equation (70) with the results of triaxial tests. It turns out from numerical calculations that the classical Cam-Clay model combined with a linear form of the NCL does not comply well with the results obtained experimentally (Figure 8). Conversely, if the bilinear NCL is involved, the evolution of the pore pressure obtained numerically coincides with the time history of pressures resulting from triaxial tests much better.

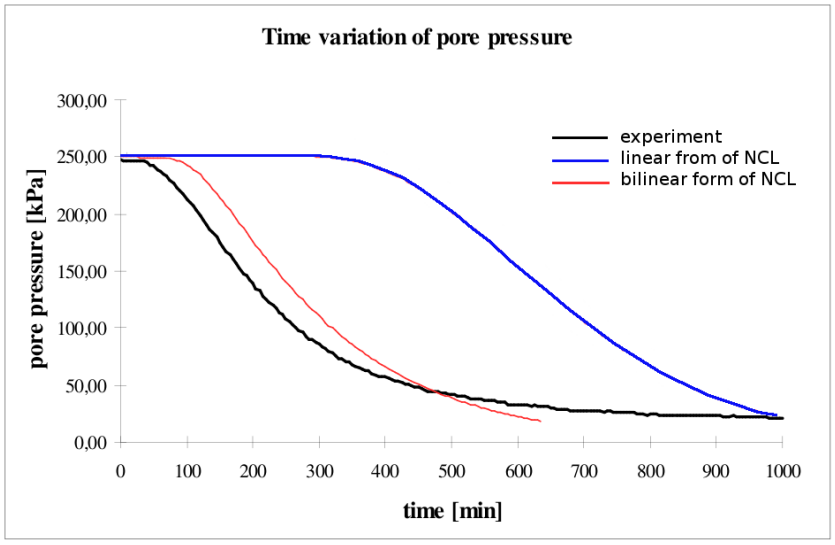

Figure 8: Time history of pore pressure (linear form of the NC line)

6 Conclusions

The numerical model describing coupled hydro-mechanical behaviour of soils was presented. Main principles of the micro-mechanics-based model based on Lewis and Schrefler's approach of heat and moisture transfer in deforming porous media was briefly described. For modelling of soil behaviour, the assumption of one-phase flow (water flow) in deforming porous medium was used in the derivation using the finite element method. The numerical model presented was implemented in the SIFEL package and tested on the simple benchmark of sand desaturation. Further, it was applied to the computer simulation of the soil consolidation process with the assumption of elastic behaviour of the soil skeleton. It was shown that the description of consolidation by the linear elastic model for a porous medium along with the constant permeability is not realistic. Therefore, the permeability variation from Cam-Clay model for modelling of cohesive soils was adopted and it will be topic of the future works The wide area of application can be found, *e.g*, in the structure - subsoil interaction influenced by changes of ground water level.

Acknowledgements

Financial support for this work was provided by GAČR project P105/11/1160. The financial support is gratefully acknowledged.

References

[1] H. M. Künzel and K. Kiessl, "Calculation of heat and moisture transfer in exposed building components", Int. J. Heat Mass Transfer, 40, 159-167, 1977.

[2] D. Gawin, C. E. Majorana, B. A. Schrefler, "Numerical analysis of hygrothermic behaviour and damage of concrete at high temperature", Mech. Cohes-Frict. Mat, 4, 37-74, 1999.

[3] J. Kočí, V. Kočí, J. Maděra, P. Rovnaníková and R. Černý, "Computational analysis of hygrothermal performance of renovation renders", Advanced Computational Methods and Experiments in Heat Transfer, XI, 267-277, 2010.

[4] R. W. Lewis and B. A., Schrefler, "The finite element method in static and dynamic deformation and consolidation of porous media", John Wiley & Sons, Chiester-Toronto, 1971.

[5] R. T. Tenchev and L. Y. Li and J. A. Purkiss, "Finite Element Analysis of Coupled Heat and Moisture Transfer in Concrete Subjected to Fire", ,Numerical Heat Transfer, 39, 685-710, 2001.

[6] T. Krejčí, T. Nový, L. Sehnoutek and J. Šejnoha, "Structure - subsoil interaction in view of transport processes in porous media", CTU Reports, 5(1), 2001.

[7] O. Rahli, F. Topin, L. Tadrist and J. Pantaloni, “Analysis of heat transfer with liquid-vapor phase change in a forced-flow fluid moving through porous media”, Int. J. Heat Mass Transfer 39, No. 18, 3959-3975, 1996.
[8] Z. P. Bazant and W. Thonguthai, “Pore pressure in heated concrete walls: theoretical prediction”, Mag. Concrete Res, 31(107), 67-76, 1979.
[9] J. R. Welty, C. E. Wicks and R. E. Wilson, “Fundamentals of heat and mass transfer”, John Wiley & Sons, New York, 1969.
[10] Z. Bittnar and J. Šejnoha, “Numerical Methods in Structural Mechanics”, ASCE Press, New York, USA, 1996.
[11] T. J. R. Hughes, “The Finite Element Method. Linear Static and Dynamic Finite Element Analysis”, Prentice-Hall, inc. Englewood Cliffs, New Jersey, 1987.
[12] A. C. Liakopoulos, “TRansient flow through unsaturated porous media”, PhD thesis, University of California, Berkeley, 1965.
[13] B. A. Schrefler and L. Simoni, “A inified approach to the analysis of saturated - unsaturated elastoplastic porous media”, Numerical Methods in Geomechanics, Balkema, Rotterdam, 205-212, 1988.
[14] O. C. Zienkiewicz, Y. M. Xie, B. A. Schrefler, A. Ledesma and N. Bicanic, “Static and dynamic behaviour of soils: a rational approach to quantitative solution, II. Semi-saturated problems”, Proc. R. Soc. Lond. A, 429, 311-321, 1990.
[15] B. A. Schrefler and Xiaoyong Zhan, “A fully coupled model for water flow and airflow in deformable porous media”, Water Resources Research, 29, 155-167. 1993.
[16] D. Gawin, and B. A. Schrefler, “Thermo-hydro-mechanical analysis of partially saturated porous materials”, Engng. Comp., 13(7), 113-143, 1996.
[17] T. Koudelka, T. Krejčí and J. Kruis, “Modeling of Building constructions in SIFEL Environment”, Czech Technical University in Prague, 2011.
[18] J. Kruis, T. Koudelka and T. Krejčí, “Multi-physics Analyses of Selected Civil Engineering Concrete Structures”, Commun. Comput. Phys., 12, 885-918, 2012.
[19] SIFEL - Simple Finite Elements, *http://mech.fsv.cvut.cz/∼sifel/index.html*.
[20] P. Kuklík, J. Mareš and M. Šejnoha, “Evaluation of the modified CAM clay model with reference to isotropic consolidation”, CTU REPORTS, 3, No. 4, 47-49, 1999.
[21] K.H. Roscoe, J.B. Burland, “ On the Generalized Stress-Strain Behavior of Wet Clay”, Engineering Plasticity, 535-609., 1968
[22] D.M. Wood, “Soil Behaviour and Critical State Soil Mechanics”, Cambridge: Cambridge University Press, 1990.
[23] J.C. Simo, M. Oritz, “A Unified Approach to Finite Deformation Elastoplasticity Based on the Use of Hyperelastic Constitutive Equations”, Computer Methods in Applied Mechanics and Engineering, 221-245, 1985
[24] M. Jirasek, Z. P. Bazant “Inelastic Analysis of Structures”, John Wiley&Sons, Ltd, Chichester, UK, 2002.
[25] E. A. de Souza Neto, D. Perić, D. R. J. Owen, “Computational Methods for Plasticity”, John Wiley&Sons, Ltd, Eastbourne, UK, 2008.